Contents lists available at ScienceDirect

Arabian Journal of Chemistry

journal homepage: www.ksu.edu.sa

Development and evaluation of rosmarinic acid loaded novel fluorescent porous organosilica nanoparticles as potential drug delivery system for cancer treatment

Uyen-Chi Nguyen Le [a], Ngoc Xuan Dat Mai [b,c], Kieu-Minh Le [d], Hoang Anh Vu [d], Huynh-Nhu Thi Tran [c,e], Tan Le Hoang Doan [b,c,*]

[a] Faculty of Basic Science, University of Medicine and Pharmacy at Ho Chi Minh City, Ho Chi Minh City, Vietnam
[b] Center for Innovative Materials and Architectures, Vietnam National University, Ho Chi Minh City, Vietnam
[c] Vietnam National University, Ho Chi Minh City, Vietnam
[d] Center for Molecular Biomedicine, University of Medicine and Pharmacy at Ho Chi Minh City, Ho Chi Minh City, Vietnam
[e] Faculty of Biotechnology, University of Science, Vietnam National University, Ho Chi Minh City, Vietnam

ARTICLE INFO

Keywords:
Fluorescent
Porous organosilica
Drug delivery
Rosmarinic acid
Cancer therapy

ABSTRACT

Rosmarinic acid is a bioactive compound that possesses high anticancer activity, but its poor water-solubility and ineffective membrane permeability are the main causes of low bioavailability. This study aimed to improve these limitations by encapsulating rosmarinic acid in tetrasulfide-based porous organosilica nanoparticles to deliver it to cancer cells. To date, no reports on the use of these organosilica nanoparticles as a nanocarrier for rosmarinic acid. The synthesized nanoparticles were small, approximately 50 nm in size, with a high surface area of around 498.1 m^2/g and an average pore diameter of 2.3 nm. Especially, fluorescent-labeled nanospheres were synthesized and further indicated the effective accumulation in the cytosol after 24 h incubation. In addition, the nanoparticles were non-toxic to human AGS gastric adenocarcinoma cells and mouse CT26 colon cancer cells within concentrations ranging from 0 to 240 μg/mL. Treatment with nanoparticles containing 140 μg/mL of rosmarinic acid resulted in the death of approximately 39.2 % of AGS cells and 36.9 % of CT26 cells after 72 h. Importantly, neither the silica nanospheres nor the rosmarinic acid-containing nanoparticles showed any significant toxic effects on HEK-293T and NIH-3T3 fibroblasts at the tested concentrations. These results suggested that the pharmacological effects of rosmarinic acid can be enhanced by encapsulating it into our novel synthesized biodegradable tetrasulfide-based porous organosilica nanoparticles.

1. Introduction

Rosmarinic acid (RA) is an ester of caffeic acid and 3,4-dihydroxyphenyl lactic acid, mostly obtained in plants belonging to the *Lamiaceae* and *Boraginaceae* families (Gordo et al., 2012). Many researchers have investigated its precious activities such as anti-inflammatory (Jiang et al., 2018), antibacterial (Jordán et al., 2012), antioxidant (Aldoghachi et al., 2021), and anticancer effects. RA affects tumorigenesis in many ways such as inhibiting tumor cell proliferation (Jang et al., 2018; Zhang et al., 2018; Shang et al., 2017; Wang et al., 2012), arresting cell cycle (Yang et al., 2018), and inducing apoptosis in cancer cells (Jang et al., 2018; Zhang et al., 2018). However, its ineffective membrane permeability results in low oral bioavailability and then limits its application as an anticancer drug (Shang et al., 2017; Wang et al., 2012; Yang et al., 2018). RA is an ionizable strong acid that influences its solubility or permeability within body fluids (Casanova et al., 2016). Through the acidic environment of the gastrointestinal tract, the stability of RA was significantly reduced (Zorić et al., 2016).

In recent years, new drug delivery systems (DDS) have been applied to improve the drug's gastrointestinal and water solubility. RA was successfully incorporated with chitosan nanoparticles (da Silva et al., 2016), solid lipid nanoparticles (Madureira et al., 2016), phospholipid complexes (Huang et al., 2019), or cyclodextrins (Aksamija et al., 2016) to improve its low bioavailability. Besides these materials,

Peer review under responsibility of King Saud University.
* Corresponding author.
E-mail address: dlhtan@inomar.edu.vn (T.L.H. Doan).

https://doi.org/10.1016/j.arabjc.2023.105402
Received 31 March 2023; Accepted 29 October 2023
Available online 1 November 2023

biodegradable porous organosilica nanoparticle (NPs) is a remarkable group of DDS that can be effectively used to encapsulate and deliver drug molecules (Lee et al., 2019; Shao et al., 2020). Specific characteristics include high specific surface area, good porosity, easy to surface modification that could increase encapsulation as well as the adjusted release profile of drug molecules. The fluorescent coating on the surface of nanoparticles gives it the ability to track in various experiments such as cellular uptake, and biodistribution in *in vivo* models (Chakkarapani et al., 2021). In our previous reports, we synthesized different types of biodegradable tetrasulfide-based porous organosilica nanoparticles and evaluated their capacity in loading some anticancer drugs like cordycepin, daunorubicin, and curcumin (Mai et al., 2020; Mai et al., 2021; Mai et al., 2021). The incorporated tetrasulfide linkers in the framework responded to redox conditions, high glutathione concentration intracellular in the tumor, and then the particle can be degraded.

In this study, we evaluated the capacity of tetrasulfide-based porous organosilica nanoparticles to retain the pharmacological effect of RA on gastrointestinal cancer cells. As with other anticancer drugs, the small nanoparticles also show high loading capacity toward RA, up to 580.1 mg/g, and specific slow-release performance. Especially, the fluorescent-labeled NPs are synthesized to evaluate their cellular uptake in various cancer cells, AGS and CT26. The results identified the cytotoxic of RA-loading NPs on human AGS gastric adenocarcinoma cells and mouse CT26 colon cancer cells. In normal human 293T cells and mouse 3T3 cells, NPs showed almost no cytotoxicity. This study may provide new insight into developing a new drug using an anticancer agent RA that is effectively delivered by nanomaterials in the patient's body.

2. Experimental

2.1. Materials

Bis[3-(triethoxysilyl) propyl] tetrasulfide, 1,2-bis(triethoxysilyl) ethane, rhodamine B isothiocyanate, rosmarinic acid, 3-(trihydroxysilyl) propyl methyl phosphonate, cell Counting Kit – 8 (CCK-8) and Annexin V-FITC apoptosis detection kit were obtained from Sigma-Aldrich. Cetyltrimethylammonium bromide (CTAB) was purchased from Thermo Fisher Scientific. Penicillin/Streptomycin, phosphate-buffered saline (PBS), fetal bovine serum (FBS), Roswell Park Memorial Institute (RPMI) 1640 medium, and Dulbecco's modified Eagle's medium (DMEM) were obtained from Invitrogen Corporation. Experimental animal cell lines were received from American Tissue and Culture Collection (ATCC).

2.2. Synthesis of nanoparticles

Tetrasulfide-based nanoparticles are synthesized as the previous reported (Mai et al., 2021). Briefly, a surfactant solution is prepared at 80 °C by combining of CTAB, water, and NaOH 1 M. After that, two silane precursors, 1,2-bis(triethoxysilyl)ethane (300 µL) and bis[3-(triethoxysilyl) propyl] tetrasulfide (100 µL), are dropwise added in turn into the surfactant solution. After 15 min, 3-(trihydroxysilyl) propyl methyl phosphonate (315 µL) is immediately added to the reaction mixture to get negatively charged particles. The condensation is kept for 105 min further at 80 °C under continuous stirring. The product is obtained using centrifugation (16000 rpm, 25 °C, 30 min) and washed twice with EtOH. The residual CTAB is removed by refluxing the obtained powder in NH_4NO_3/EtOH solution. NPs sample is centrifugated and washed with EtOH and DI water followed by vacuum activated at 80 °C for 24 h. The Rhodamine B isothiocyanate-labeled NPs were synthesized by post-synthesized. Briefly, a RITC stock solution was prepared by stirring overnight (400 rpm, room temperature) a mixture of RITC (5 mg), ethanol (5 mL), and 3-aminotriethoxysilane (20 µL). 20 mg synthesized-NPs was immersed in 20 mL EtOH and further added 1 mL RITC stock solution. The mixture was stirred for 24 h at room temperature. Finally, the fluorescent NPs were collected by centrifugation and washed several times with water.

2.3. Characterization of nanoparticles

Scanning electron microscope (SEM) images and transmission electron microscope (TEM) images are obtained using an S4800 microscope (Hitachi Ltd., Tokyo, Japan) and a JEM-2100 microscope (JEOL Ltd., Japan), respectively. Elemental analyses (EA) were performed by using a Eurovector EA3100 elemental analyzer. A Bruker Vertex 70 FT-IR spectrometer is used for Fourier transform infrared (FT-IR) spectra. Thermal gravimetric analysis (TGA) is measured on a Q-500 thermogravimetric analyzer (TA Instruments, Tokyo, Japan). The UV–Vis spectra were collected on a JASCO V-770 spectrophotometer. The temperature is increased from room temperature to 800 °C (a heating rate of 5 °C/minute) under continuous airflow. The N_2 adsorption isotherms are obtained at 77 K via a Quantachrome Autosorb iQ2 (Quantachrome Instruments, Florida, USA). The measurement is operated using liquid nitrogen and under ultrahigh-purity-grade N_2 and He. Dynamic light scattering were analyzed by Zetasizer Nano ZS (Malvern, UK) to evaluate the stability and zeta potential of nanoparticles.

2.4. Drug loading

RA loading experiment is based on the adsorption equilibrium method (Zhao et al., 2016). NPs are dispersed in 1 mL of RA solution (0.75 mg/mL). The loading is conducted by stirring at room temperature for 24 h at 600 rpm. Rosmarinic acid-loaded nanoparticles (RA@NPs) are collected by centrifugation (14,000 rpm/30 min). The supernatant is analyzed in high-performance liquid chromatography (HPLC). HPLC is equipped with a Thermal Scientific Hypersil BDS-C18 column (4.6 × 150 mm, 5 µm) on the Shimadzu LC-40D XR series HPLC systems. The mobile phase is 92.5 methanol: 2.5 formic acid: 5 water (v/v). The separation was conducted at 30 °C at 330 nm. The injected volume is 20 µL with a flow rate of 0.75 mL/min.

The RA loading capacity (mg/g) is determined via the following formulas:

$$\text{Loading capacity} = \frac{(m_o - m_r)}{m}$$

where m_o is the initial RA weight (mg); m_r is the unloaded-RA weight (mg); m is the NPs weight (g).

2.5. In vitro drug release

A dialysis bag diffusion technique is applied to evaluate the release profile (He et al., 2017). Briefly, RA@NPs are dispersed in phosphate-buffered saline/DMSO (9:1) (pH 5.5 and pH 7.4) and followed by transferring to a dialysis bag (MW cut off = 14 kDa, Sigma-Aldrich) to be immersed in respectively release solution. The system is shaken at 37 °C. The supernatant (200 µL) was taken at the predetermined time intervals and the fresh solution (200 µL) was supplemented into the system. The collected supernatants are analyzed using HPLC to determine release profiles.

2.6. Cell culture

Human gastric adenocarcinoma (AGS, CRL-1739) and mouse colon carcinoma (CT26, CRL-2638) cell lines are cultured in RPMI 1640 medium. Human embryonic kidney (293T, CRL-3216) and mouse embryonic fibroblast (3T3, CRL-1658) cell lines are cultured in a DMEM medium. The complete culture media are supplemented with 10 % FBS and 1 % Penicillin/Streptomycin. Cells are routinely maintained in the log phase in a humidified incubator with 5 % CO_2 at 37 ℃.

2.7. Cell uptake

For cellular uptake assay, $3x10^3$ cells (AGS or CT26) were prepared in each well of an 8-well chamber slide overnight. Cells were incubated with 120 μg/mL of RITC-labeled NPs for 24 h, then fixed with 4% formaldehyde in PBS. Images were acquired with an Eclipse T12 confocal microscope [Nikon Corp., Tokyo, Japan] with excitation and emission at 544 nm and 612 nm, respectively.

2.8. Cell viability assay

Measurement of cell viability is determined using CCK-8 assay as previously described (Mai et al., 2021). Briefly, cells are seeded in 96-well plates at a density of 3×10^3 cells per well and treated with different concentrations of test compounds: RA (17.5, 35, 70, and 140 μg/mL), NPs (30, 60, 120, and 240 μg/mL), RA@NPs (contains 17.5, 35, 70, and 140 μg/mL of RA with correlative NPs weight at 30, 60, 120, and 240 μg/mL). The untreated cells are considered as a control group. After 24 h of treatment, cells are washed and further cultured for 48 h in complete media. Then, 10 μL of CCK-8 solution is added to each well and incubated for 2 h. The absorbance is measured using a microplate reader IRE96 (SFRI, France) at 450 nm. All tests are triplicated. The percent of cell viability ratio (CVR) is calculated based on the following formula:

$$\text{CVR}\,(\%) = \frac{OD_s x100}{OD_o}$$

where OD_s: optical density of sample.

OD_o: optical density of control.

To examine the abnormality of cell morphology, cells are visualized and photographed directly using a phase-contrast inverted microscope Eclipse TS100 (Nikon Corp., Tokyo, Japan) before performing the CCK-8 assay.

2.9. Annexin V-fluorescein isothiocyante (FITC)/Propidium iodide (PI) apoptosis assay

Apoptosis assay was performed using an Annexin V-FITC apoptosis detection kit (Sigma-Aldrich, St. Louis, MO, USA). Briefly, AGS and CT26 cells were treated with 240 μg/mL of RA@NPs (contains 140 μg/mL of RA) or 140 μg/mL of RA for 24 h, followed by a 48 h incubation in new media. The untreated cells are considered as control groups. All cells were harvested and washed two times with cold PBS. After centrifugation, the cell pellet was resuspended and stained with 5 μL Annexin V-FITC and 10 μL PI. The flow cytometry analysis was performed within 15 min. The test was duplicated.

2.10. Statistical analyses

All data are analysed by Microsoft Exel and expressed as mean ± standard deviation (SD). The statistical analyses are carried out by Anova for comparisons between two samples using GraphPad prism 7 software. The values are considered significant at $^*P < 0.05$, $^{**}P < 0.01$ and $^{***}P < 0.001$.

3. Results and discussion

3.1. Characterization of silica nanoparticles

We synthesized the tetrasulfide-based porous organosilica nanoparticles by the sol–gel method as previous description (Mai et al., 2021). The morphological uniform nanosized spheres are obtained via the SEM image with an average particle diameter of about 50 nm (Fig. 1A). Furthermore, as depicted in Fig. 1B, nanoparticle size is distributed in a narrow area with an average size of approximately 52 nm. In addition, the TEM images confirmed the spherical particles which corresponded with SEM images. The particle size is approximately 50 nm (Fig. S1). Furthermore, the shape and size of nanoparticles after loading with rosmarinic acid drug were not changed (Fig. S1B).

To determine the functional linkers in the nanoparticles, FT-IR analysis was conducted. It can be seen in Fig. 2A, the very broad peak around 3460 cm^{-1} corresponded to the hydroxyl group stretching frequency on the surface of silica materials. The successful condensation of precursors is demonstrated via the Si-O-Si stretching band at 1034–1160 cm^{-1}. The presence of tetrasulfide-linker in the structure is obtained via the C-S stretching bands at 694 cm^{-1}, respectively. In addition, NPs showed peaks at 1634 cm^{-1} which is attributed to O–H bending vibrations of water molecule on the particles surface. All the peaks obtained are well matched with previous results (Mai et al., 2020; Mai et al., 2021).

In addition, thermogravimetric analysis is conducted to further determine the composition of nanoparticles. It can be seen in Fig. 2B, the small amount of weight of the particles is decomposed until 100 °C which is responding to the adsorption of solvent and water in the porous structures. A large amount of material, nearly 30 %, is strongly decomposed from 200 to 700 °C. That reduction is responded to the organic composition, ethane- and tetrasulfide-moieties, in the silica framework. That confirmed the successful incorporation of biodegradable linkers.

Nitrogen adsorption–desorption isotherm is obtained to evaluate the porosity of nanoparticles. The isotherm showed a mesoporous structure of the nanoparticle due to type IV isotherm (Fig. 2C). Furthermore, the Barrett-Joyner-Halenda (BJH) average pore diameter and the calculated

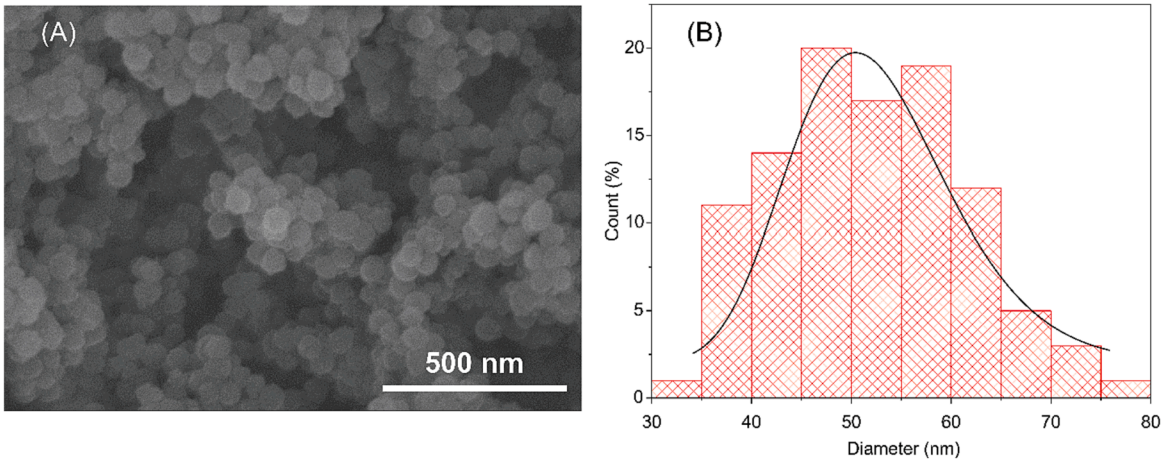

Fig. 1. (A) Scanning electron micrograph of the nanoparticles. (B) Particle size distribution calculated by ImageJ software.

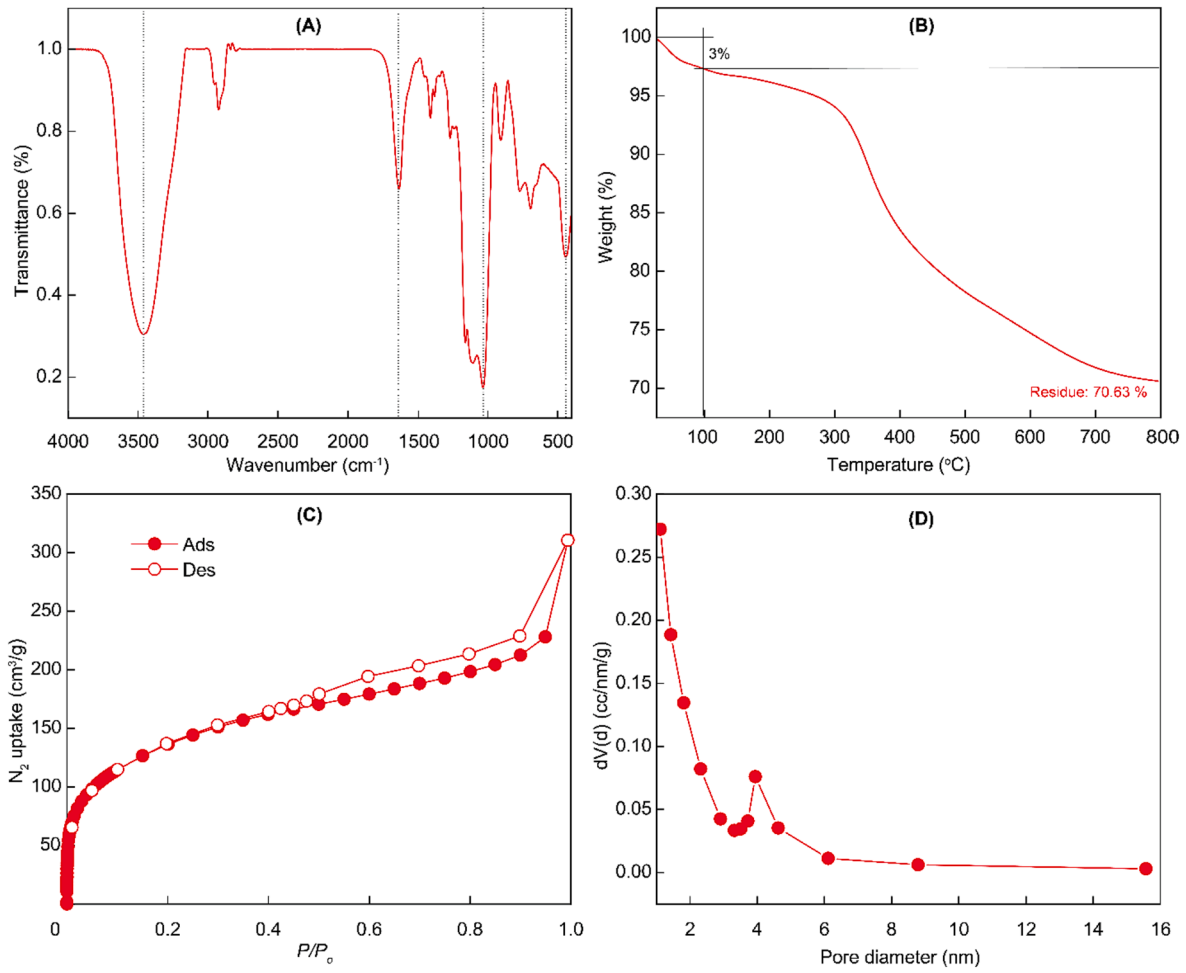

Fig. 2. Characterizations of nanoparticles. (A) FT-IR spectrum. (B) Thermogravimetric analysis under air condition. (C) nitrogen adsorption–desorption isotherm under 77 K. (D) Barrett-Joyner-Halenda pore distribution.

Brunauer-Emmett-Teller (BET) surface area of the nanoparticle was approximately 2.3 nm and 498.1 m^2/g, respectively (Fig. 2D). The performance of nanoparticles is affected by their stability. As shown in Fig. S2, NPs showed stability with similar particle size and insignificant differences in count rate. After 6 h, a slight decrease in count rate, approximately 10 %, indicating the high stability of particles. These obtained results guarantee the capacity to load drug molecules including rosmarinic acid.

3.2. The cellular uptake into cancer cells of RITC-labeled NPs

As a property of nanomaterials, the ability of the synthetic 50 nm NPs to be absorbed into the cell, corresponding to the ability of this material to deliver drugs into the cell, is a matter of demonstration. NPs were attached with red luminescent RITC compound to facilitate the observation of the particles by fluorescence microscopy. Merged confocal microscopic images of AGS and CT26 cells (Fig. 3) showed that RITC-labeled NPs 50 nm in size were internalized into cells. Several studies reported that the MSNs definitely could accumulate in cells (Lu et al., 2009) by both passive diffusion and active endocytotic pathway, then distribute freely in cytoplasma or within lysosomal compartments (Zhu et al., 2013; Li et al., 2016; Hu et al., 2011). Moreover, cellular uptake is highly particle-size-dependent with the optimal size of particles for cell uptake being 50 nm (Lu et al., 2009; Jiang et al., 2008).

3.3. Rosmarinic acid loading capacity of nanoparticles and its release profiles

The RA loading capacity of NPs was evaluated via HPLC analysis. Results showed that the loading capacity was 580.1 mg/g. It is interesting that the zeta potential of the original nanoparticles was increased significantly after loading with RA molecules (Fig. 4A). The zeta potential of the negative charge of pristine nanoparticles was around − 24.96 mV. In contrast, its zeta potential is increased to − 13.53 mV which demonstrated the successful encapsulation of rosmarinic acid into the structures. We assumed that the hydroxyl group in RA molecules strongly interacted with the abundant hydroxyl group on the surface of nanoparticles resulting in the increase of zeta potential.

From the releasing profile in Fig. 4B, the released RA rose stepwise meantime but in low doses. At the point of 1 h, released RA amounts were 5.4 % at pH 5.5, 6.4 % at pH 6.4 and 8.0 % at pH 7.4; then reached about 10.1 %, 10.8 % and 11.0 % at 48 h, respectively. We assumed that these amounts could be RA which is attached to the nanoparticle surface. Meanwhile, free RA is released higher in the same conditions. The lower RA amount released from NPs over a long time indicated the capacity of NPs to prevent RA molecules from early release and then increase their efficiency at the targeted sites. Hence, NPs can safely deliver drugs in the low pH distributing route of the digestive system or tumor extracellular space (pH 6.4–7.0), avoiding the loss of a certain drug amount before its delivery into tumor cells (Hao et al., 2018). These results indicated the slow-release performance of NPs towards RA molecules.

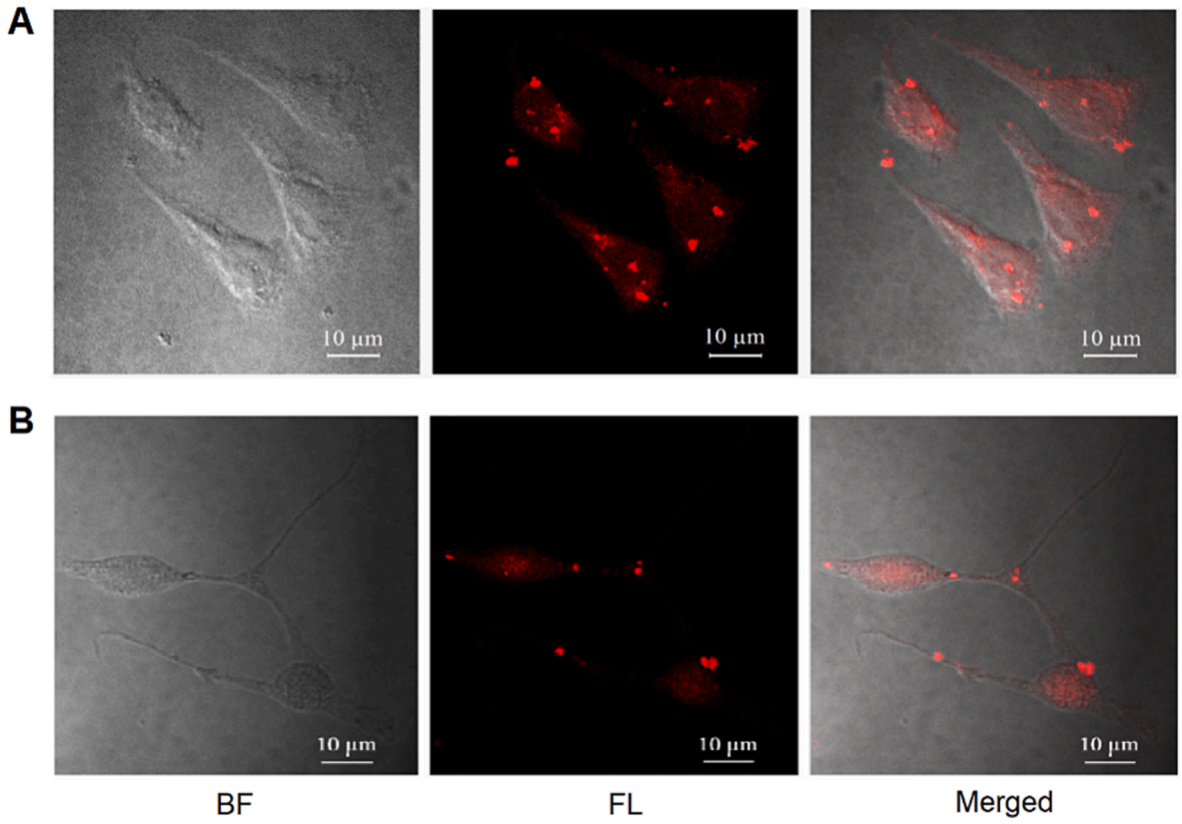

Fig. 3. The uptake of NPs in cancer cells. (A) AGS cells and (B) CT26 cells were cultured with RITC-labeled NPs (100 μg/mL) for 24 h. Bright field (BF), fluorescence (FL) and merged images were captured by a confocal fluorescence microscope with magnification x600. Scale bar 10 μm.

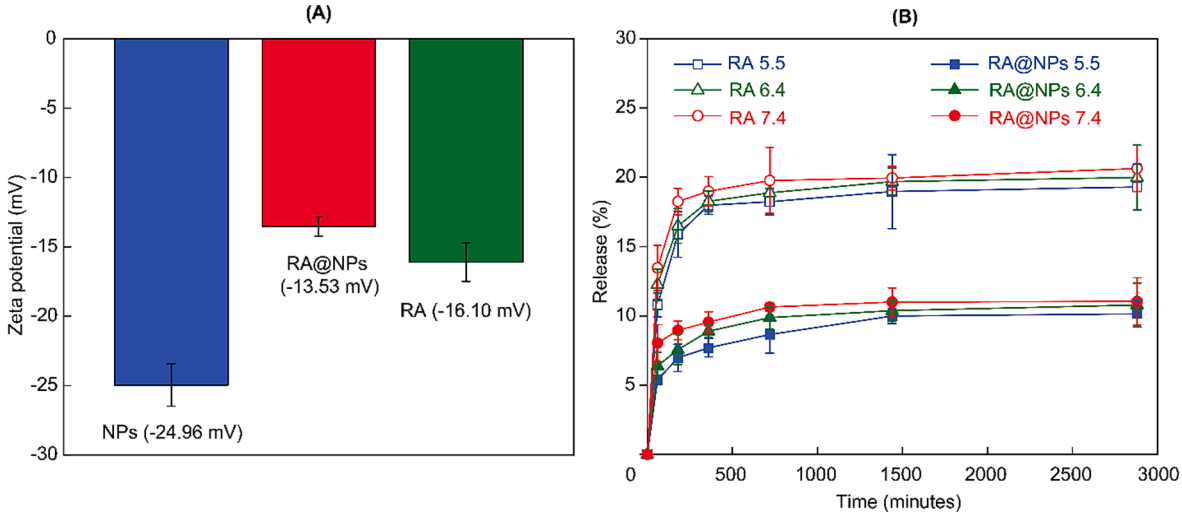

Fig. 4. (A) Zeta potential of NPs, RA and RA-loaded NPs. (B) Release profile of RA@NPs at various pH.

3.4. RA@NPs inhibited cancer cell survival

The CCK-8 assay on two cancer cell lines (gastric cancer AGS and colon cancer CT26) and two normal cell lines (kidney 293T and fibroblast 3T3) were performed to evaluate the ability to enhance the activity of RA-loading silica nanoparticles.

Results showed that the cytotoxicity was induced on AGS and CT26 cell lines treated with either RA or RA@NPs when using drug concentrations from 35 μg/mL to 140 μg/mL (Fig. 5A-B). This cytotoxicity was dose-dependent, in the same manner as other *in vitro* studies on silica nanoparticles (Li et al., 2011; Shi et al., 2010; Wilczewska et al., 2012). Using RA@NPs (140 μg/mL), the minimum percentages of CVR induced in AGS and CT26 cells were 60.8 % and 63.1 %, respectively.

The cytotoxicity was not seen in NPs-treated groups on all cell types when using low concentrations (0–60 μg/mL). Higher concentration of NPs (240 μg/mL) caused a slight decrease in cell survival percentage in CT26 cells (87.5 ± 3.6 %), AGS cells (89.2 ± 1.9 %), 293T cells (91.1 ± 2.4 %), and 3T3 cells (92.7 ± 3.5 %). The toxicity of silica particles seems to be dependent on the cell line (Blechinger et al., 2013). Toxicity studies of nanosilica materials show that toxicity is directly proportional to material dose and treatment time (Li et al., 2011; Wilczewska et al., 2012). The longer the contact time, the more the material will increase

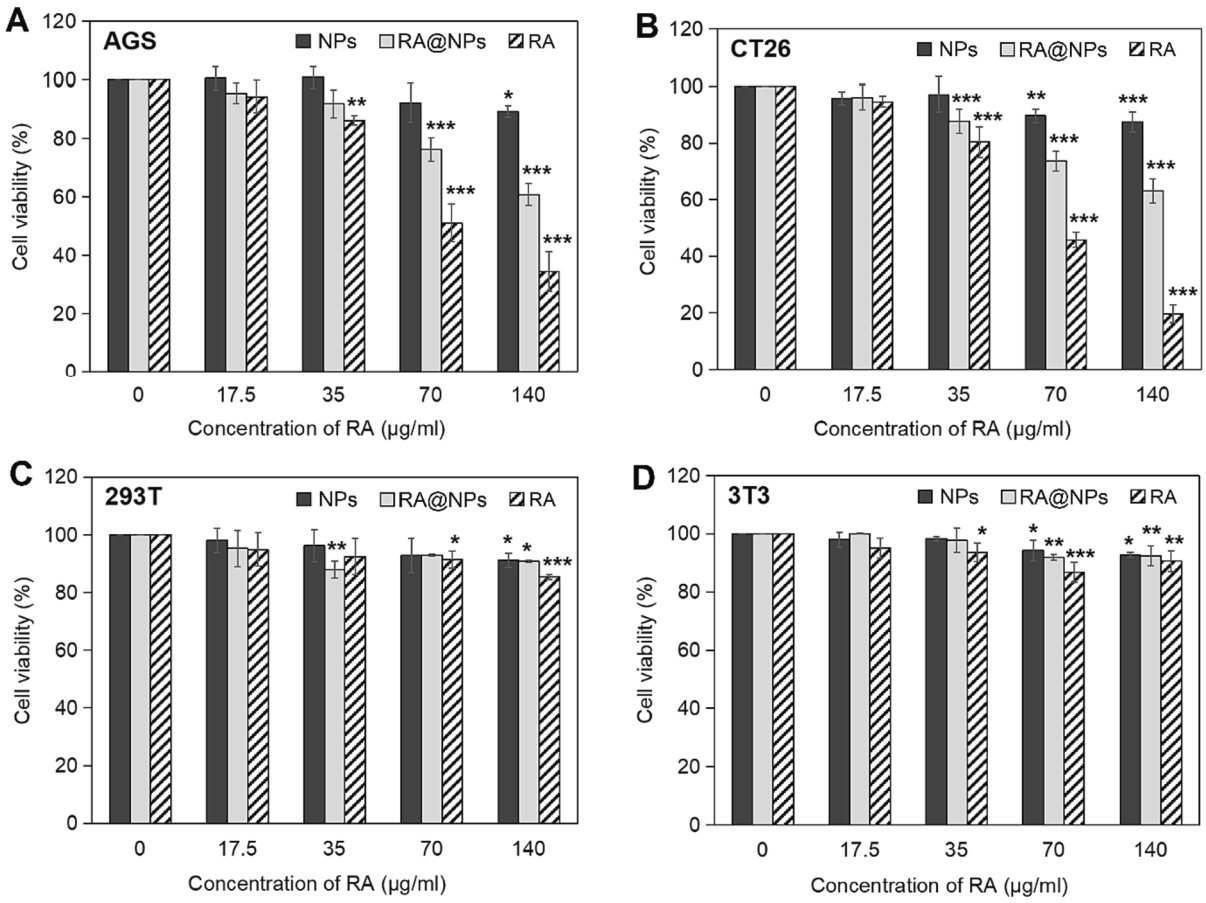

Fig. 5. Cytotoxicity analysis of RA@NPs on cells by CCK-8 assay. (A) AGS cells; (B) CT26 cells; (C) 293T cells; (D) 3T3 cells. Cells were treated with NPs, RA@NPs, or RA for 24 h and further incubation for 48 h. The experiments are conducted independently three times and data are presented as their mean ± SD. P value was calculated at different doses vs. control. *P < 0.05, **P < 0.01, ***P < 0.001.

the cell-particle interaction and the particle's cellular uptake capacity. At a high dose of treatment, the toxicities of 50 nm NPs in two cancer cell lines were more serious than those in normal cells. Slight toxicity from other 50 nm silica nanoparticles was demonstrated toward the human L-02 hepatocytes for 72 h (Lu et al., 2011), in human bronchial epithelial cell lines (HBEC3-KT and BEAS-2B) with ~ 10–25 % of cell viability (Låg et al., 2018), or even no cytotoxicity on primary human umbilical vein endothelial cells (Corbalan et al., 2011).

In addition, by comparing the CVRs of AGS and CT26 cancer cells treated with NPs and RA@NPs, we supposed that the effective cytotoxicity was generated due to the activity of RA compounds which might be released from porous pores. For example, in AGS cells, the CVR % of the NPs-treated group (89.2 %) was higher compared to the CVR% of the RA@NPs-treated group (60.8 %), as well as in CT26 cells, those values were 87.5 % (of NPs-treated group) and 63.1 % (of RA@NPs-treated group).

Noted that the effect of RA@NPs was not as effective as that of RA (Fig. 5A-B). In AGS cells incubated with 240 μg/mL of RA@NPs (containing 140 μg/mL of RA) or 140 μg/mL of RA, the percentage of alive cells were 60.8 % and 34.5 %, respectively. Similarly, in CT26 cells treated with 240 μg/mL of RA@NPs (containing 140 μg/mL of RA) or 140 μg/mL of RA, the CVR% were 63.1 % and 19.7 %, respectively. We assumed that the Sigma commercial polyphenolic RA compound, derived from *Rosmarinus officinalis* L., can be completely soluble in water up to 1 mg/mL of final concentration and consequently inhibit cancer cell survival more quickly and effectively at a high concentration within 72 h. As in this study, although RA@NPs are less cytotoxic than RA, they have the ability to preserve and release drugs slowly (Fig. 4B), meeting the standards of a DDS. In this study, we utilized biodegradable tetrasulfide-linker NPs as carriers in order to stabilize and prolong the activity of RA, because of their high biocompatibility and low bioaccumulation as compared with the undegradable nanoparticles (Croissant et al., 2017). Here, the NPs have been proved to be completely degraded after 7 days in 10 mM glutathione/PBS solution (Mai et al., 2021). This biodegradable ability of NPs results from the cleavage of -S-S- linker in the porous structure (Mai et al., 2020; Chen et al., 2014; Huang et al., 2017; Huang et al., 2013). The potential to protect and gradually release RA of NPs might lead to the postponement in RA activity to suppress the proliferation of AGS and CT26 cells within 72 h of incubation.

Cancer cell survival was also visualized by inverted microscopy (Fig. 6). At 72 h post-treatment with RA@NPs (240 μg/mL nanoparticles contain 140 μg/mL of RA) or with RA solution (140 μg/mL), there were not many adherent living cells with a normal shape attached to the bottom of the culturing wells. In contrast, many dead cells were usually suspended in a culture medium and had abnormal morphologies such as spherical and swelling bodies (yellow arrow), or shrinkage and budding forms (red arrow), which were considered as apoptotic cells (Lu et al., 2011; Han et al., 2015).

Moreover, the Annexin V-FITC/PI staining assay revealed the magnitude of the apoptosis generated by RA and RA@NPs treatment. The kit uses annexin V combined with FITC to label phosphatidylserine sites on the membrane surface at early-stage apoptosis and PI for labeling cellular DNA in necrotic cells where the cell membrane has been completely damaged. This combination allows differentiation between early apoptotic cells (annexin V positive, PI negative), late apoptotic cells (annexin V positive, PI positive), necrotic cells (annexin V negative, PI positive) and surviving cells (annexin V negative, PI negative). Almost

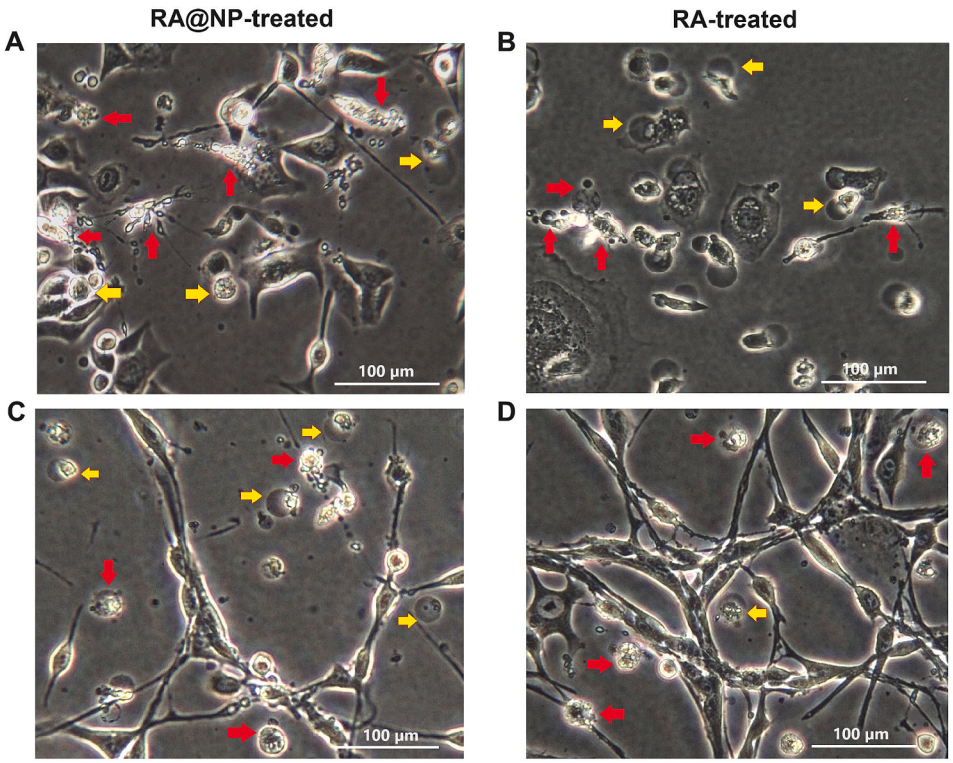

Fig. 6. Cell death morphology visualized under phase-contrast microscope. (A-B) AGS cells and (C-D) CT26 cells were treated with RA@NPs and RA at concentration of 140 µg/mL for 72 h. Arrows point to dead cells with abnormal morphological changes. Scale bar 100 µm.

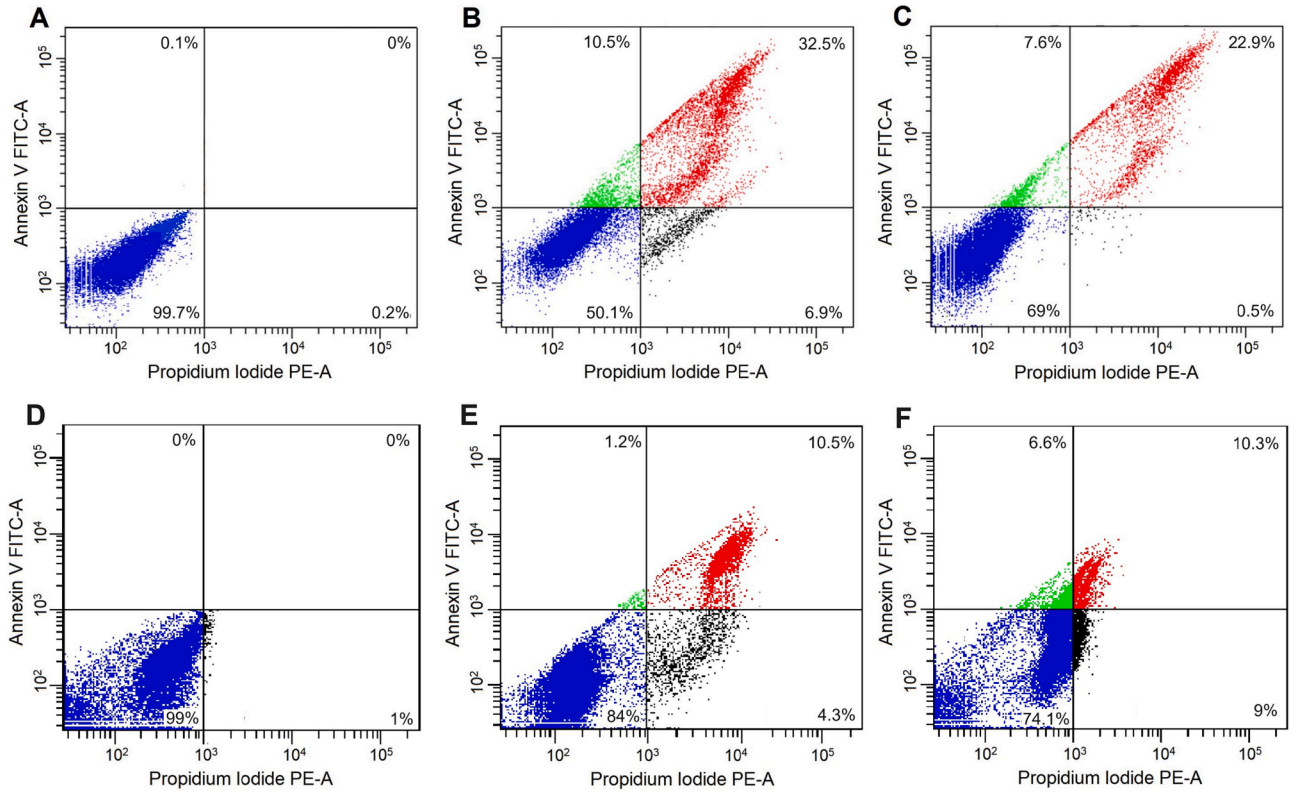

Fig. 7. Flow cytometry analysis of cancer cells using Annexin V-FITC/PI staining. (A-C) AGS and (D-F) CT26 cells were incubated with RA@NPs (B, E) or RA (C, F). The untreated cells are control groups (A, D). Viable cells (lower left square), early apoptotic cells (upper left square), late apoptotic cells (upper right square) and necrotic cells (lower right square).

cancer cells were survival in control groups (Fig. 7A, D); meanwhile, many apoptotic cells could be found in both the RA and RA@NPs treated groups. The number of AGS cells undergoing apoptosis by RA@NPs and RA treatment were 43 % and 30.5 % (Fig. 7B-C), respectively, and the corresponding numbers in CT26 cell apoptosis were 11.7 % and 16.9 % (Fig. 7E-F). These results demonstrated that the new synthesized RA@NP materials could induce apoptosis in both AGS and CT26 cancer cells.

4. Conclusions

The bioavailability of rosmarinic acid - a herbal bioactive compound - should be enhanced for further medical applications in cancer treatment therapy. Here, we first time incorporated RA into tetrasulfide-based porous organosilica nanoparticles as a drug delivery system and examined its anticancer activity *in vitro*. The synthesized nanoparticle showed uniform spherical shapes with an average size is around 50 nm. Their chemical composition and high porosity were also demonstrated. Especially, fluorescent-labeled NPs were synthesized for evaluating the cellular uptake of materials. This nanoparticle also expressed a high loading capacity of rosmarinic acid, reaching 580.1 mg/g with slow-release profiles. The findings of the apoptosis-related cytotoxic effects of RA@NPs on AGS and CT26 cell lines offer a promising potential for the development and application of this material in the medicinal treatment of gastrointestinal cancer diseases.

CRediT authorship contribution statement

Uyen-Chi Nguyen Le: Conceptualization, Methodology, Validation, Writing – original draft, Writing – review & editing, Supervision, Project administration, Funding acquisition. **Ngoc Xuan Dat Mai:** Conceptualization, Methodology, Formal analysis, Validation, Writing – original draft. **Kieu-Minh Le:** Conceptualization, Formal analysis. **Hoang Anh Vu:** Conceptualization, Formal analysis, Validation. **Huynh-Nhu Thi Tran:** Conceptualization, Formal analysis, Validation, Writing – original draft. **Tan Le Hoang Doan:** Conceptualization, Methodology, Formal analysis, Validation, Writing – review & editing.

Declaration of competing interest

The authors declare that they have no known competing financial interests or personal relationships that could have appeared to influence the work reported in this paper.

Acknowledgements

This research is funded by University of Medicine and Pharmacy at Ho Chi Minh City, Viet Nam under grant number 06/2020/HĐ-ĐHYD. We would like to thank Assoc. Prof. Binh Thanh Nguyen for performing confocal microscopy. The authors express their sincere thanks to the Center for Innovative Materials & Architectures (INOMAR), Viet Nam National University, Ho Chi Minh City for their support in using the nitrogen adsorption-desorption isotherm, FT-IR, and TGA measurements.

Appendix A. Supplementary material

Supplementary data to this article can be found online at https://doi.org/10.1016/j.arabjc.2023.105402.

References

Aksamija, A., Polidori, A., Plasson, R., Dangles, O., Tomao, V., 2016. The inclusion complex of rosmarinic acid into beta-cyclodextrin: A thermodynamic and structural analysis by NMR and capillary electrophoresis. Food Chem. 208, 258–263.

Aldoghachi F, UM NA-M, Shari F (2021) Antioxidant Activity of Rosmarinic Acid Extracted and Purified from Mentha piperita. Arch Razi Inst 76(5):1279.

Blechinger, J., Bauer, A.T., Torrano, A.A., Gorzelanny, C., Bräuchle, C., Schneider, S.W., 2013. Uptake kinetics and nanotoxicity of silica nanoparticles are cell type dependent. Small 9 (23), 3970–3980.

Casanova, F., Estevinho, B., Santos, L., 2016. Preliminary studies of rosmarinic acid microencapsulation with chitosan and modified chitosan for topical delivery. Powder Techol. 297, 44–49.

Chakkarapani, S.K., Shin, T.H., Lee, S., Park, K.-S., Lee, G., Kang, S.H., 2021. Quantifying intracellular trafficking of silica-coated magnetic nanoparticles in live single cells by site-specific direct stochastic optical reconstruction microscopy. J. Nanobiotechnol. 19 (1), 1–15.

Chen, Y., Meng, Q., Wu, M., Wang, S., Xu, P., Chen, H., Li, Y., Zhang, L., Wang, L., Shi, J., 2014. Hollow mesoporous organosilica nanoparticles: a generic intelligent framework-hybridization approach for biomedicine. J. Am. Chem. Soc. 136 (46), 16326–16334.

Corbalan, J.J., Medina, C., Jacoby, A., Malinski, T., Radomski, M.W., 2011. Amorphous silica nanoparticles trigger nitric oxide/peroxynitrite imbalance in human endothelial cells: inflammatory and cytotoxic effects. Int. J. Nanomed. 6, 2821.

Croissant, J.G., Fatieiev, Y., Khashab, N.M., 2017. Degradability and clearance of silicon, organosilica, silsesquioxane, silica mixed oxide, and mesoporous silica nanoparticles. Adv. Mater. 29 (9), 1604634.

da Silva, S.B., Ferreira, D., Pintado, M., Sarmento, B., 2016. Chitosan-based nanoparticles for rosmarinic acid ocular delivery—*In vitro* tests. Int. J. Biol. Macromol. 84, 112–120.

Gordo J, Máximo P, Cabrita E, Lourenço A, Oliva A, Almeida J, Filipe M, Cruz P, Barcia R, Santos M, and Cruz H (2012) Thymus mastichina: chemical constituents and their anti-cancer activity. Nat Prod Commun 7(11):1934578X1200701120.

Han, S., Yang, S., Cai, Z., Pan, D., Li, Z., Huang, Z., Zhang, P., Zhu, H., Lei, L., Wang, W., 2015. Anti-Warburg effect of rosmarinic acid via miR-155 in gastric cancer cells. Drug Des. Devel. Ther. 9, 2695–2703.

Hao, G., Xu, Z.P., Li, L., 2018. Manipulating extracellular tumour pH: an effective target for cancer therapy. RSC Adv. 8 (39), 22182–22192.

He, Y., Liang, S., Long, M., Xu, H., 2017. Mesoporous silica nanoparticles as potential carriers for enhanced drug solubility of paclitaxel. Mater. Sci. Eng. C 78, 12–17.

Hu, L., Mao, Z., Zhang, Y., Gao, C., 2011. Influences of size of silica particles on the cellular endocytosis, exocytosis and cell activity of HepG2 cells. J. Nanosci. Lett. 1.

Huang, P., Chen, Y., Lin, H., Yu, L., Zhang, L., Wang, L., Zhu, Y., Shi, J., 2017. Molecularly organic/inorganic hybrid hollow mesoporous organosilica nanocapsules with tumor-specific biodegradability and enhanced chemotherapeutic functionality. Biomaterials 125, 23–37.

Huang, J., Chen, P.X., Rogers, M.A., Wettig, S.D., 2019. Investigating the phospholipid effect on the bioaccessibility of rosmarinic acid-phospholipid complex through a dynamic gastrointestinal *in vitro* model. Pharmaceutics 11 (4), 156.

Huang, L., Lu, Y., Guo, S., Yang, J., Liang, Z., Zhang, Q., Yi, P., Feng, Y., Li, Y., Xu, Y., Qiu, X., Feng, J., Shen, Z., 2013. A strategy of limited-space controlled aggregation for generic enhancement of drug loading capability. Adv. Funct. Mater. 33 (4), 2209278.

Jang, Y.-G., Hwang, K.-A., Choi, K.-C., 2018. Rosmarinic acid, a component of rosemary tea, induced the cell cycle arrest and apoptosis through modulation of HDAC2 expression in prostate cancer cell lines. Nutrients 10 (11), 1784.

Jiang, W., Kim, B., Rutka, J.T., Chan, W.C., 2008. Nanoparticle-mediated cellular response is size-dependent. Nat. Nanotechnol. 3 (3), 145–150.

Jiang, K., Ma, X., Guo, S., Zhang, T., Zhao, G., Wu, H., Wang, X., Deng, G., 2018. Anti-inflammatory effects of rosmarinic acid in lipopolysaccharide-induced mastitis in mice. Inflamm. 41 (2), 437–448.

Jordán, M.J., Lax, V., Rota, M.C., Lorán, S., Sotomayor, J.A., 2012. Relevance of carnosic acid, carnosol, and rosmarinic acid concentrations in the *in vitro* antioxidant and antimicrobial activities of Rosmarinus officinalis (L.) methanolic extracts. J. Agric. Food Chem. 60 (38), 9603–9608.

Låg, M., Skuland, T., Godymchuk, A., Nguyen, T.H., Pham, H.L., Refsnes, M., 2018. Silica nanoparticle-induced cytokine responses in BEAS-2B and HBEC3-KT cells: significance of particle size and signalling pathways in different lung cell cultures. Basic Clin. Paharmacol. Toxicol. 122 (6), 620–632.

Lee, S.H., Park, O.K., Kim, J., Shin, K., Pack, C.G., Kim, K., Ko, G., Lee, N., Kwon, S.H., Hyeon, T., 2019. Deep tumor penetration of drug-loaded nanoparticles by click reaction-assisted immune cell targeting strategy. J. Am. Chem. Soc. 141 (35), 13829–13840.

Li, Y., Sun, L., Jin, M., Du, Z., Liu, X., Guo, C., Li, Y., Huang, P., Sun, Z., 2011. Size-dependent cytotoxicity of amorphous silica nanoparticles in human hepatoma HepG2 cells. Toxicol. *in Vitro* 25 (7), 1343–1352.

Li, Y., Yu, Y., Duan, J., Li, Z., Geng, W., Jiang, L., Wang, J., Jin, M., Liu, X., Sun, Z., 2016. The internalization, distribution, and ultrastructure damage of silica nanoparticles in human hepatic L-02 cells. Part. Part. Syst. Char. 33 (9), 664–674.

Lu, X., Qian, J., Zhou, H., Gan, Q., Tang, W., Lu, J., Yuan, Y., Liu, C., 2011. *In vitro* cytotoxicity and induction of apoptosis by silica nanoparticles in human HepG2 hepatoma cells. Int. J. Nanomed. 6, 1889.

Lu, F., Wu, S.H., Hung, Y., Mou, C., 2009. Size effect on cell uptake in well-suspended, uniform mesoporous silica nanoparticles. Small 5 (12), 1408–1413.

Madureira, A.R., Campos, D.A., Oliveira, A., Sarmento, B., Pintado, M.M., Gomes, A.M., 2016. Insights into the protective role of solid lipid nanoparticles on rosmarinic acid bioactivity during exposure to simulated gastrointestinal conditions. Colloids Surf. B 139, 277–284.

Mai, N.X.D., Birault, A., Matsumoto, K., Ta, H.K.T., Intasa-ard, S.G., Morrison, K., Thang, P.B., Doan, T.L.H., Tamanoi, F., 2020. Biodegradable periodic mesoporous organosilica (BPMO) loaded with daunorubicin: a promising nanoparticle-based anticancer drug. ChemMedChem 15 (7), 593–599.

Mai, N.X.D., Dang, Y.T., Ta, H.K.T., Bae, J.-S., Park, S., Phan, B.T., Tamanoi, F., Doan, T. L.H., 2021. Reducing particle size of biodegradable nanomaterial for efficient curcumin loading. J. Mater. Sci. 56 (5), 3713–3722.

Mai, N.X.D., Le, U.-C.-N., Nguyen, L.H.T., Ta, H.T.K., Van Nguyen, H., Le, T.M., Phan, T. B., Nguyen, L.-T.-T., Tamanoi, F., Doan, T.L.H., 2021. Facile synthesis of biodegradable mesoporous functionalized-organosilica nanoparticles for enhancing the anti-cancer efficiency of cordycepin. Microporous Mesoporous Mater. 315, 110913.

Shang, A.-J., Yang, Y., Wang, H.-Y., Tao, B.-Z., Wang, J., Wang, Z.-F., Zhou, D.-B., 2017. Spinal cord injury effectively ameliorated by neuroprotective effects of rosmarinic acid. Nutr. Neurosci. 20 (3), 172–179.

Shao, D., Zhang, F., Chen, F., Zheng, X., Hu, H., Yang, C., Tu, Z., Wang, Z., Chang, Z., Lu, J., Li, T., Zhang, Y., Chen, L., Leong, K.W., Dong, W.F., 2020. Biomimetic diselenide-bridged mesoporous organosilica nanoparticles as an X-ray-responsive biodegradable carrier for chemo-immunotherapy. Adv. Mater. 32 (50), e2004385.

Shi, Y., Yadav, S., Wang, F., Wang, H., 2010. Endotoxin promotes adverse effects of amorphous silica nanoparticles on lung epithelial cells *in vitro*. J. Toxicol. Environ. Health Part A 73 (11), 748–756.

Wang, J., Xu, H., Jiang, H., Du, X., Sun, P., Xie, J., 2012. Neurorescue effect of rosmarinic acid on 6-hydroxydopamine-lesioned nigral dopamine neurons in rat model of Parkinson's disease. J. Mol. Neurosci. 47 (1), 113–119.

Wilczewska, A.Z., Niemirowicz, K., Markiewicz, K.H., Car, H., 2012. Nanoparticles as drug delivery systems. Pharmacol. Rep. 64 (5), 1020–1037.

Yang, J.-H., Mao, K.-J., Huang, P., Ye, Y.-J., Guo, H.-S., Cai, B.-C., 2018. Effect of piperine on the bioavailability and pharmacokinetics of rosmarinic acid in rat plasma using UPLC-MS/MS. Drug Metab. Pharmacokinet. 48 (2), 178–185.

Zhang, Y., Hu, M., Liu, L., Cheng, X.-L., Cai, J., Zhou, J., Wang, T., 2018. Anticancer effects of Rosmarinic acid in OVCAR-3 ovarian cancer cells are mediated via induction of apoptosis, suppression of cell migration and modulation of lncRNA MALAT-1 expression. J. B.U.ON. 23 (3), 763–768.

Zhao, Z., Gao, Y., Wu, C., Hao, Y., Zhao, Y., Xu, J., 2016. Development of novel core-shell dual-mesoporous silica nanoparticles for the production of high bioavailable controlled-release fenofibrate tablets. Drug Dev. Ind. Pharm. 42 (2), 199–208.

Zhu, J., Liao, L., Zhu, L., Zhang, P., Guo, K., Kong, J., Ji, C., Liu, B., 2013. Size-dependent cellular uptake efficiency, mechanism, and cytotoxicity of silica nanoparticles toward HeLa cells. Talanta 107, 408–415.

Zorić, Z., Markić, J., Pedisić, S., Bučević-Popović, V., Generalić-Mekinić, I., Grebenar, K., Kulišić-Bilušić, T., 2016. Stability of rosmarinic acid in aqueous extracts from different Lamiaceae species after *in vitro* digestion with human gastrointestinal enzymes. Food Technol. Biotechnol. 54 (1), 97–102.